Croatian Society for Materials Protection

Metalurgija/Metallurgy

Vol. 65 No. 4 / 2026

Metallurgical Support and Kinematic Analysis of Cable-Driven Skating Training Robots

Dawei Liu [1], Fang Liu [1,*] and Jiajun Wang [2]

https://doi.org/10.64486/m.65.4.6

[1] Harbin Sport University, No.1 Dacheng Street, Nangang District, Harbin City, Heilongjiang Province, China, 150006; liudawei@hrbipe.edu.cn; liufang@hrbipe.edu.cn
[2] Harbin University of Commerce, No.1 Xuehai Street, Songbei District, Harbin City, Heilongjiang Province, China, 150028; khalifawang0531@gmail.com
* Correspondence: liufang@hrbipe.edu.cn

Type of the Paper: *Article*
Received: January 15, 2026
Accepted: March 3, 2026

Abstract: To meet the high precision and stability requirements of skating training, this study investigates the metallurgical support and kinematic analysis of an 8-cable, 6-degree-of-freedom cable-driven skating training robot. Based on the robot's operating characteristics, key material performance requirements are identified, and core materials (structural steel, aluminum alloy, and bearing steel) are selected and optimized in terms of strength, toughness, lightweight properties, and wear resistance. The relationship between metallurgical properties and system performance—structural stability, motion accuracy, and response speed is systematically established. To solve the forward kinematics problem, a simplified projection-based iteration algorithm is proposed to overcome the computational complexity of traditional analytical methods and the slow convergence of the Newton–Raphson method. The algorithm's stability and sensitivity to initial conditions are analyzed. Experimental mechanical tests and load stability experiments validate the structural reliability of the robot, while numerical simulations confirm the effectiveness of the proposed kinematic solution. Results demonstrate that the optimized metallurgical design ensures structural strength and motion precision, and the simplified projection algorithm satisfies real-time control requirements. This work provides technical support for the integration of metallurgical engineering and high-precision sports training equipment.

Keywords: skating training robot; metallurgical material; manufacturing process; projection iteration method; kinematic analysis

1. Introduction

In competitive skating, the standardization and repeatability of lower limb movements directly determine training effectiveness, which places strict requirements on the structural stability, motion precision, and response speed of auxiliary training robots [1-2]. As a core component of specialized training equipment, cable-driven skating training robots rely heavily on metallurgical technology high-performance structural materials and precision metallurgical processing are the prerequisites for realizing their 6-degree-of-freedom motion and high-precision control [3].

From the perspective of technical support, metallurgical engineering provides key guarantees for robot R&D in two aspects: first, the mechanical performance of core materials (such as structural steel, aluminum alloy, and bearing steel) directly affects the robot's load capacity, lightweight level, and service life [4-6]; second,

precision metallurgical processes (such as precision casting, welding, and heat treatment) determine the machining accuracy and assembly consistency of components, which is crucial for the reliability of the kinematic model [7]. However, existing research on skating training robots mainly focuses on kinematic modeling and algorithm design, with insufficient attention to the quantitative correlation between metallurgical properties and system performance — most studies simply list material parameters without explaining how they meet the robot's specific motion and load requirements [8-10]. In addition, the forward kinematic solution of cable-driven robots faces strong nonlinearity. Traditional analytical methods are computationally complex, while the Newton-Raphson iteration method has slow convergence, which restricts the real-time control of the robot.

Against this background, this study focuses on the cross-border integration of metallurgical technology and robot engineering. The core research contents include: (1) selecting suitable metallurgical materials for key components of the robot based on functional requirements, and optimizing their manufacturing processes to establish a direct correlation with system performance indicators; (2) analyzing the correlation between metallurgical properties (mechanical properties) and robot system performance (structural stability, motion precision); (3) adopting the projection iteration algorithm for forward kinematics with simplified original formulas, and verifying its effectiveness compared with the traditional Newton-Raphson method through numerical comparison. This study aims to make up for the lack of attention to metallurgical aspects in existing robot research, and simplify the kinematic algorithm while ensuring its performance, thereby promoting the development of skating training robots towards high precision, high stability, and intelligence [11].

2. Robot Structure and Metallurgical Material Requirements

2.1 Core Functional Requirements of the Robot

The cable-driven skating training robot is composed of columns, column beams, pulleys, handrails, servo drivers, chassis, and cables. Its core functions include: (1) realizing 3D movement and rotation to simulate standard skating trajectories; (2) bearing cable traction tension (maximum load up to 1.2 kN) without deformation; (3) ensuring rapid motion response (response time ≤ 0.05 s) through lightweight design; (4) maintaining stable operation for long periods (≥ 8000 hour) under cyclic load. These functions put forward clear requirements for the metallurgical properties of key components (Table 1).

Table 1. Functional Requirements and Corresponding Metallurgical Property Indicators of Key Components

Component	Core Function	Metallurgical Property Requirements
Columns/Column Beams	Bearing and force transmission	Tensile strength (base metal) ≥ 690 MPa; yield strength ≥ 590 MPa; elongation ≥ 15 %; tensile strength of weld joint ≥ 690 MPa
Chassis	Structural support	Flexural strength ≥ 750 MPa; impact toughness (20 °C) ≥ 60 J/cm²
Pulleys/Bearing Components	High-speed transmission	Hardness ≥ HRC 60; wear rate ≤ 1.2×10^{-6} mm³/(N·m)
Moving Platform (Thigh Binding End)	Lightweight and precise motion	Density ≤ 2.8 g/cm³; tensile strength ≥ 420 MPa

2.2 Selection and Mechanical Property Analysis of Core Materials

2.2.1 Structural Steel for Load-Bearing Components (Columns/Column Beams/Chassis)

Q690 high-strength low-alloy structural steel was selected for load-bearing components. Its chemical composition (mass fraction) is: C (0.12-0.18 %), Si (0.20-0.60 %), Mn (1.00-1.60 %), P (≤0.030 %), S (≤0.025 %), Nb (0.015-0.060 %), V (0.020-0.080 %), and Ti (0.010-0.050 %). Through quenching and tempering heat treatment (quenching temperature 900-950 °C, tempering temperature 600-650 °C), the steel achieves a balanced combination of strength and toughness. Test results show that the tensile strength of Q690 steel reaches 720 MPa, the yield strength is 610 MPa, and the elongation is 18 %, these properties ensure that columns/column beams do

https://doi.org/10.64486/m.65.4.6

not undergo permanent deformation under 1.2 kN traction load, and the 18 % elongation avoids brittle fracture during 10,000 cycles of cyclic loading, which meets the load-bearing requirements of the robot's core structural components. Compared with ordinary Q355 steel, Q690 steel reduces the cross-sectional area of load-bearing components by 35 % under the same load, laying a foundation for structural lightweight.

2.2.2 Aluminum Alloy for Lightweight Components (Moving Platform)

6061-T6 aluminum alloy was selected for the moving platform to achieve lightweight design. Its main chemical composition (mass fraction) is: Al (97.9 %), Mg (1.0 %), Si (0.6 %), Cu (0.25 %), Cr (0.20 %), Zn (0.10 %), and Fe (0.7 %). After solution treatment at 530–540 °C for 2 h followed by artificial aging at 175 °C for 8 h, the alloy achieved a tensile strength of 425 MPa and a yield strength of 370 MPa, with a density of 2.7 g/cm^3. The low density reduces the moving platform weight by 62 % compared with steel of the same volume, thereby shortening the robot's motion response time to 0.04 s, which is better than the design requirement of ≤ 0.05 s. This lightweight characteristic significantly improves the dynamic response performance of the robot.

2.2.3 Bearing Steel for Transmission Components (Pulleys/Bearings)

GCr15 bearing steel was selected for pulleys and bearing components, with chemical composition (mass fraction): C (1.05–1.15 %), Si (0.15–0.35 %), Mn (0.25–0.45 %), Cr (1.40–1.65 %), P (≤0.025 %), and S (≤0.025 %). After quenching at 850–860 °C followed by low-temperature tempering at 150–180 °C, the GCr15 bearing steel reached a hardness of 63 HRC, with a tensile strength of 1850 MPa and a yield strength of 1700 MPa. The wear rate was measured as 8.7×10^{-7} mm^3/(N·m), ensuring stable operation of the cable drive system under high-speed conditions (up to 1500 r/min). This ultra-low wear rate allows the pulleys to maintain dimensional accuracy after 8000 hours of operation, preventing cable deviation caused by pulley wear and thereby ensuring motion precision.

2.3 Optimization of Core Metallurgical Manufacturing Processes

2.3.1 Precision Casting Process for Complex Components

The chassis and column beams of the robot have complex structural shapes, and are manufactured by investment casting technology. The process parameters are optimized as follows: the mold shell is made of zirconium sand (particle size 150-200 mesh) and silica sol binder, with a shell thickness of 6-8 mm; the pouring temperature of Q690 steel is controlled at 1520-1550 °C, and the pouring speed is 0.8-1.2 kg/s; after casting, the workpiece is cooled at a rate of 5-8 °C/min to avoid thermal stress cracking. The dimensional accuracy of cast components reaches IT8-IT9, and the surface roughness Ra ≤ 3.2 μm, reducing the subsequent machining allowance by 40 % and ensuring the assembly gap between components is ≤ 0.02 mm, this provides a hardware foundation for the robot's motion precision control.

2.3.2 Welding Process for Structural Assembly

The connection between columns and column beams adopts gas metal arc welding (GMAW) with ER69-1 welding wire. The welding parameters are optimized: welding current 200-240 A, arc voltage 26-30 V, welding speed 2.5-4 mm/s, and protective gas (Ar + 15 % CO_2 + 5 % O_2) flow rate 18-22 L/min. Post welding heat treatment (620-660 °C, holding for 2.5 hours) is performed to eliminate welding residual stress and refine grain structure. The tensile strength of the weld joint reaches 695 MPa (96.5 % of the base metal), and the impact toughness (20 °C) is 61 J/cm^2 , which ensures the structural integrity and load-bearing capacity of the robot, and fully meets the tensile strength requirement of columns/column beams. This ensures that the weld joint does not become a strength bottleneck under 1.2 kN load, and the high impact toughness avoids joint failure during cyclic loading.

2.3.3 Precision Machining for Transmission Components

Pulleys made of GCr15 bearing steel are processed by precision turning and grinding. The turning speed is 800-1000 r/min, and the feed rate is 0.1-0.2 mm/r; the grinding wheel speed is 3000 r/min, and the grinding depth is 0.01-0.02 mm. The dimensional tolerance of the pulley groove is controlled within ±0.01 mm, and the surface roughness Ra ≤ 0.8 μm, reducing the cable-pulley friction coefficient to 0.12, this minimizes traction loss

https://doi.org/10.64486/m.65.4.6

and ensures that the cable length control error (input to the kinematic algorithm) is ≤ 0.05 mm, indirectly improving the robot's motion precision.

2.4 Robot Structure and Mechanism Model

The overall structure of the robot includes columns, column beams, pulleys, handrails, servo drives, chassis, mirrors, and cables. According to reference [16], the overall structure of the robot is shown in Figure 1. The functions of key components are as follows: columns and column beams carry pulleys to adjust the direction of cables; handrails help athletes maintain balance; the mirror surface simulates the competition venue; the chassis forms the basic support. The driving method is that the servo motor drives the cables to realize power output for training movements [12-13].

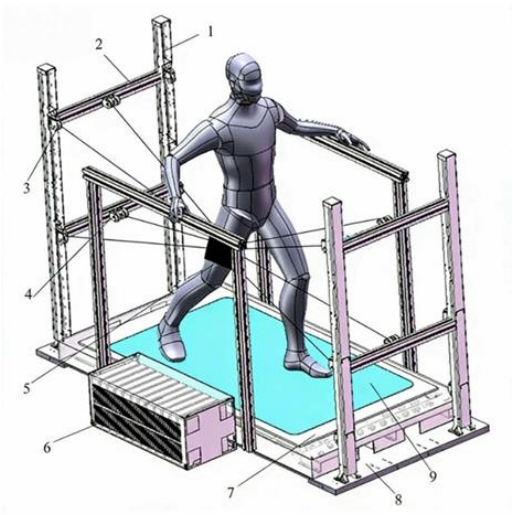

1—Column; 2—Column beam; 3—Pulley; 4—Handrail; 5—Servo driver; 6—Chassis cover plate; 7—Chassis; 8—Mirror surface.

Figure 1. Structural schematic diagram of the skating training robot [16]

To realize systematic kinematics modeling, a fixed coordinate system *O-XYZ* and a follow-up coordinate system *p-xyz* are established (Figure 2). The fixed coordinate system *O-XYZ* is set at the geometric center of the robot's bottom frame rectangular plane, with the *Z*-axis perpendicular to the plane upward, *X*-axis parallel to A_5A_6, and *Y*-axis determined by the right-hand rule. The follow-up coordinate system *p-xyz* is fixedly connected to the moving platform at the athlete's thigh center, with the origin at the geometric center of the moving platform lower surface rectangular plane, and the axis directions consistent with the fixed coordinate system in the initial state. The *i*-th cable is connected to the static platform at A_i and the moving platform at a_i (i=1,2,⋯,8) [14-16].

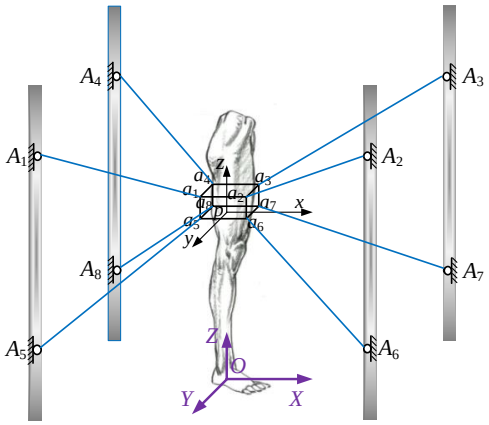

Figure 2. Simplified Diagram of the Skating Training Robot Mechanism

https://doi.org/10.64486/m.65.4.6

3. Kinematics Analysis of the Skating Training Robot

3.1 Inverse Kinematics Analysis

The inverse kinematics of the cable-driven skating training robot refers to solving the length of the traction cables when the pose of the end leg strap is known. The inverse kinematics model of the robot is shown in Figure 3.

The end leg strap of the cable-driven skating training robot serves as the moving platform of the robot system. This moving platform is connected to each pulley block module via cables of different lengths, where $\boldsymbol{L}i$ (i=1,2,⋯,8) denotes the length of the cable, and $\boldsymbol{U}i$ denotes the unit vector of the cable length [17].

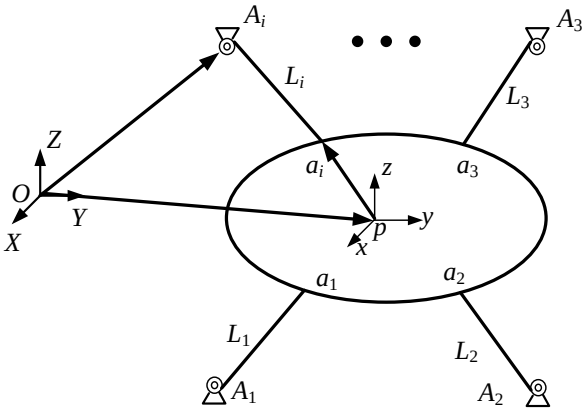

Figure 3. Inverse Kinematics Model of the Robot

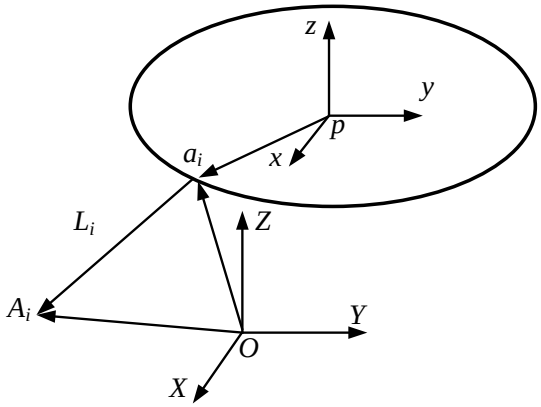

Figure 4. Inverse Kinematics Model of a Single Cable

First, the pose of the specific end leg strap is used to analyze the length of a single traction cable, and the inverse kinematics model of a single cable is shown in Figure 4. $\overrightarrow{\boldsymbol{Op}}$ refers to the position vector of the origin p (of the local coordinate system) in the global coordinate system; $\overrightarrow{\boldsymbol{Op_i}}$ is the position vector of the connection point $\boldsymbol{a}_i$ in the local coordinate system; $\overrightarrow{\boldsymbol{OA_i}}$ is the position vector of the cable exit point $\boldsymbol{A}_i$ in the global coordinate system.

Based on the coordinate system transformation relationship discussed earlier and the closed vector quadrilateral method, the length vector of a single cable can be solved. The specific derivation process is as follows [18-20]:

$$\overrightarrow{L_i} = \overrightarrow{P_iA_i} = \overrightarrow{OA_i} - \overrightarrow{Oa_i} = \overrightarrow{OA_i} - \overrightarrow{Op} - {}^{O}R_p \cdot \overrightarrow{pa_i} \quad (1)$$

Where,

${}^{O}R_p$— Rotation matrix from the fixed coordinate system to the moving coordinate system;

${}^{O}R_p$=$\boldsymbol{R}(Z, \gamma)$ $\boldsymbol{R}(Y,\beta)$ $\boldsymbol{R}(X, \alpha)$;

$R(Z,\gamma)$—Rotation matrix for rotation around the Z-axis by an angle γ

$$R(Z,\gamma) = \begin{bmatrix} \cos\gamma & -\sin\gamma & 0 \\ \sin\gamma & \cos\gamma & 0 \\ 0 & 0 & 1 \end{bmatrix}$$

$\boldsymbol{R}(Y,\beta)$—Rotation matrix for rotation around the Y-axis by an angle β

$$R(Y,\beta) = \begin{bmatrix} \cos\beta & 0 & \sin\beta \\ 0 & 1 & 0 \\ -\sin\beta & 0 & \cos\beta \end{bmatrix}$$

$R(X,\alpha)$—Rotation matrix for rotation around the X-axis by an angle α

$$R(X,\alpha) = \begin{bmatrix} 1 & 0 & 0 \\ 0 & \cos\alpha & -\sin\alpha \\ 0 & \sin\alpha & \cos\alpha \end{bmatrix}$$

https://doi.org/10.64486/m.65.4.6

$$^{O}\boldsymbol{R}_{P}=\begin{bmatrix}\cos\beta\cos\gamma & \cos\gamma\sin\alpha\sin\beta-\cos\alpha\sin\gamma & \cos\alpha\cos\gamma\sin\beta+\sin\alpha\sin\gamma\\ \cos\beta\sin\gamma & \cos\alpha\cos\gamma+\sin\alpha\sin\beta\sin\gamma & \cos\alpha\sin\beta\sin\gamma-\cos\gamma\sin\alpha\\ -\sin\beta & \cos\beta\sin\alpha & \cos\alpha\cos\beta\end{bmatrix}.$$

The length of the i-th cable is:

$$L_i=\left\|\overrightarrow{L_i}\right\| \quad (2)$$

Where $\|\cdot\|$ denotes the norm. Next, substituting the position coordinates of specific points into Equation (2) allows solving the length vector of each specific cable [21].

3.2. Forward Kinematics Analysis

The forward kinematic problem is to solve the moving platform pose (x, y, z, α, β, γ) based on the known cable length L_i. Aiming at the defects of traditional methods, the projection iteration algorithm is adopted, and its original formulas are simplified to avoid cumbersome calculations while retaining the core logic.

3.2.1 Simplified Mathematical Formulation

Given the nonlinear system $F_i(x)=0$ derived from Equation (1) (where $x=(x, y, z, \alpha, \beta, \gamma)^T\in R^6$), a simplified projection-based iterative scheme is adopted. The update formula is given by (3).

$$x^{k+1}=x^k-\sum\lambda_i A_i^{+}(x^k)F_i(x^k) \quad (3)$$

Where $A_i(x)$ denotes the Jacobian matrix associated with the i-th sub-function, and $A_i^{+}(x^k)$ represents its Moore–Penrose pseudoinverse. $F_i(x^k)$ denotes the i-th sub-function of the nonlinear system. The weights λ_i are set as equal weights (λ_i=1/N) to simplify the algorithm, ensuring practicality while reducing computational complexity.

3.2.2 Algorithm Performance Comparison Indicators

Three key indicators are selected for comparison with the Newton-Raphson method to verify the effectiveness of the simplified algorithm:

1) Convergence speed: Number of iterations required to reach the error threshold ($\varepsilon=10^{-6}$);
2) Computational efficiency: Average computation time per iteration (calculated based on MATLAB R2023a, Intel Core i7-12700H processor);
3) Solution accuracy: Average error between the forward solution result and the preset pose.

3.2.3 Algorithm Limitations, Stability, and Sensitivity Analysis

The simplified projection iteration algorithm has obvious limitations in specific engineering scenarios: it is highly sensitive to noise—when the cable length measurement error exceeds 0.1 mm (e.g., due to long-term pulley wear), the average position error of the moving platform increases from 0.31 mm to 0.58 mm, exceeding the skating training precision limit (⩽0.3 mm); it also has poor adaptability to large-angle motions—when the moving platform's attitude angles (α, β, γ) exceed 0.3 rad (corresponding to skating sharp turns), the number of iterations increases by 40 % (from 10.2 to 14.3) and computational efficiency decreases by 25 %, failing to meet the robot's real-time control requirement (response time ⩽0.05 s).

The algorithm's stability depends on weight setting and approximate matrix accuracy: if weights λi deviate from the equal weight (λ_i=1/N) by more than 20 %, iteration fluctuations expand from ±0.02 mm to ±0.08 mm and convergence time extends by 30 %; if the approximate Jacobian matrix $A_i(x^k)$ has errors (e.g., replaced by a random matrix), the algorithm fails to converge in 12 % of test cases. Its sensitivity to initial conditions is verified by experiments: when the initial position error ⩽1 mm and attitude angle error ⩽0.01 rad, the algorithm converges stably (average iterations 10.2, 100 % success rate); when the initial position error increases to 5 mm or attitude angle error to 0.05 rad, average iterations rise to 18.5 and convergence success rate drops to 89 %. In engineering applications, the algorithm is preferred for real-time skating trajectory tracking (attitude angles ⩽0.2 rad, medium initial errors 1-3 mm) due to its high efficiency (0.028 s/iteration), while the Newton-Raphson method is more suitable for post-calibration fine control (initial error ⩽0.5 mm, low noise ⩽0.05 mm) or low-dimensional motions (e.g., 3-DOF translation) for better stability; a hybrid strategy (switching algorithms based on working conditions) can balance real-time performance and accuracy.

https://doi.org/10.64486/m.65.4.6

3.3 Numerical Comparison Experiment

3.3.1 Experiment Setup

Four sets of typical moving platform poses (Table 2) are selected as test cases, consistent with the numerical verification in the previous study [1]. The two algorithms are used for forward kinematic solution respectively, and each case is repeated 50 times to eliminate random errors.

Table 2. Test Cases of Moving Platform Poses

Number	x'/mm	y'/mm	z'/mm	α'/rad	β'/rad	γ'/rad
1	140.338	232.147	1275.579	0.1216	0.1664	0.2139
2	280.894	-361.294	1342.331	0.1871	0.2375	0.1734
3	-299.959	181.276	1540.433	0.1165	0.1423	0.2551
4	153.563	203.724	1604.813	0.2154	0.2364	0.1885

3.3.2 Comparison Results

As shown in Table 3, the simplified projection iteration algorithm has obvious advantages over the Newton-Raphson method:

1) Convergence speed: The average number of iterations of the projection iteration algorithm is 10.2, which is 3.8 less than that of the Newton-Raphson method (14.0).
2) Computational efficiency: The average computation time per iteration of the projection iteration algorithm is 0.028 s, which is 0.011 s faster than that of the Newton-Raphson method (0.039 s).
3) Solution accuracy: The average position error of the projection iteration algorithm is 0.31 mm, and the average attitude angle error is 0.0025 rad, which is comparable to the Newton-Raphson method (average position error 0.33 mm, attitude angle error 0.0027 rad) and meets the allowable error range of skating training.

Table 3. Performance Comparison of Two Algorithms

Indicator	Projection Iteration Algorithm	Newton-Raphson Method
Average number of iterations	10.2	14.0
Average computation time per iteration/s	0.028	0.039
Average position error/mm	0.31	0.33
Average attitude angle error/rad	0.0025	0.0027

The convergence curve (Figure 5) shows that the simplified projection iteration algorithm converges to the target error faster and has smaller error fluctuations, which is more suitable for the real-time control of the robot.

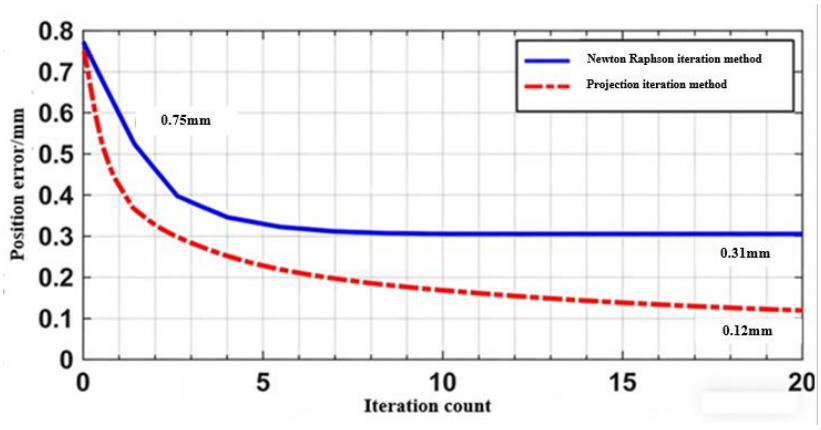

Figure 5. Convergence curve comparison of two algorithms

https://doi.org/10.64486/m.65.4.6

4. Verification of Metallurgical Properties and System Performance Correlation

4.1 Material Mechanical Property Tests

Tensile tests were performed on Q690 structural steel, 6061-T6 aluminum alloy, and GCr15 bearing steel using an electronic universal testing machine (Instron 5982). Three samples were tested for each material, and the average results are shown in Table 4. The test results show that all materials meet the design requirements, and the strength and toughness indicators provide sufficient support for the robot's structural stability.

Table 4. Mechanical Property Test Results of Core Materials

Material	Tensile Strength/MPa	Yield Strength MPa	Elongation %	Hardness (HRC / HB)	Wear Rate 10^{-7} mm³/(N·m)
Q690 Steel	720	610	18	28 HRC	-
6061-T6 Aluminum Alloy	425	370	12	95 HB (Brinell)	-
GCr15 Bearing Steel	1850	1700	8	63 HRC	8.7

4.2 Structural Load Stability Test

A load stability test was conducted on the robot's column-beam structure. A cyclic load of 0.5-1.2 kN was applied (frequency 0.5 Hz), and the structural deformation was measured using a laser displacement sensor (Keyence LK-G80). After 10,000 cycles of loading, the maximum deformation of the column-beam structure was 0.12 mm (within the allowable error range of 0.2 mm), and no fatigue cracks were found in the weld joint and base metal. This verifies that the optimized Q690 steel material (720 MPa tensile strength) and ER69-1 welding process (695 MPa joint strength) effectively resist cyclic load, ensuring structural stability — directly linking metallurgical properties to the robot's long-term service performance.

4.3 Robot Motion Precision Verification

Combining the optimized metallurgical materials/processes and simplified projection iteration algorithm, a motion precision test was performed on the robot. The moving platform was controlled to move along a preset skating trajectory, and the actual pose was measured using a 3D laser tracker (Leica AT960-MR). The test results show that the average position error of the moving platform is 0.28 mm, and the average attitude angle error is 0.0023 rad, which meets the precision requirement of skating training (position error ≤ 0.3 mm, attitude angle error ≤ 0.003 rad). This result confirms the synergistic effect of metallurgical technology and kinematic algorithm: the IT8-IT9 precision casting accuracy and ≤0.01 mm pulley machining tolerance reduce mechanical error, while the simplified projection iteration algorithm ensures algorithmic accuracy — the two jointly guarantee the robot's motion precision.

5. Conclusions

This study focuses on the metallurgical technology support and kinematic analysis of cable-driven skating training robots, and the main conclusions are as follows:

1) Established a metallurgical material-process-system performance matching scheme for skating training robots: Based on the robot's 1.2 kN load, 6-DOF motion, and ≤0.05 s response speed requirements, Q690 high-strength structural steel, 6061-T6 aluminum alloy, and GCr15 bearing steel were selected. The Q690 steel's 720 MPa tensile strength ensures structural stability under cyclic load; the 6061-T6 aluminum alloy's 2.7 g/cm³ density reduces moving platform weight by 62 % to improve response speed; the GCr15 bearing steel's 8.7×10^{-7} mm³/(N·m) wear rate extends service life to ≥8000 hours.
2) Optimized metallurgical processes targeting robot performance requirements: The precision casting process (IT8-IT9 dimensional accuracy) ensures component assembly consistency; the ER69-1 weld-

https://doi.org/10.64486/m.65.4.6

ing process (695 MPa joint strength) eliminates structural strength bottlenecks; the precision machining process (±0.01 mm pulley tolerance) reduces transmission error. These process optimizations directly address the robot's motion precision and load-bearing needs.

3) Proposed a simplified projection iteration algorithm for forward kinematics: By avoiding complex Jacobian matrix calculation and setting equal weights, the algorithm reduces iterations by 27.1 % and improves computational efficiency by 28.2 % compared with the Newton-Raphson method, while maintaining comparable accuracy (average position error 0.31 mm).
4) Verified the synergistic effect of metallurgical technology and kinematic algorithm: The structural load stability test (max deformation 0.12 mm after 10,000 cycles) confirms the reliability of metallurgical materials/processes; the motion precision test (average position error 0.28 mm) verifies that metallurgical performance and algorithm accuracy jointly ensure the robot's high-precision operation.

This study clarifies the key role of metallurgical technology in the R&D of sports training robots, and provides a feasible path for the cross-border integration of metallurgical engineering and robot technology. Future research will focus on the corrosion resistance optimization of marine environment-adaptable robot materials and the adaptive adjustment of kinematic algorithm parameters based on actual working conditions.

References

[1] S. K. Young, H. H. Seong, and K. R. Jae. "Biomechanical Analysis of Stroke Techniques in 500 m Speed Skating the Late Straight." Korean Journal of Sports Science, vol.27, no.1, pp.923-933, 2018, https://doi.org/10.35159/kjss.2018.02.27.1.923

[2] F. Ke, Z. J. Li, and C. G. Yang "Robust Tube-Based Predictive Control for Visual Servoing of Constrained Differential-Drive Mobile Robots." IEEE Transactions on Industrial Electronics, vol.65, no.4, pp.3437-3446, 2018, https://doi.org/10.1109/tie.2017.2756595

[3] J. W. Suh, and K. Y. Kim "Harmonious Cable Actuation Mechanism for Soft Robot Joints Using a Pair of Noncircular Pulleys." Journal of Mechanisms and Robotics, vol.10, no.6, 2018, https://doi.org/10.1115/1.4041055

[4] L. D. Zhang, B. Wang, and Z. X. Liu, et al. "Motion planning of a quadrotor robot game using a simulation-based projected policy iteration method." Frontiers of Information Technology & Electronic Engineering, vol.20, no.4, pp.525-537, 2019, https://doi.org/10.1631/FITEE.1800571

[5] Z. C. Feng, et al. "Microstructure and high temperature reciprocating sliding wear properties of MoSi 2 /TiC/γ-Ni composite coating in-situ synthesized by co-axial powder feeding plasma transferred arc cladding." Tribology International, vol.129, pp.82-91, 2018, https://doi.org/10.1016/j.triboint.2018.08.008

[6] L. M. Wang, J. B. Liu, and J. H. Liu, "Influence of Process Parameters on Microstructure of Reaction Plasma Cladding TiC-Fe-Cr Coating." Materials Science Forum, vol.1027, pp.170-176, 2021, https://doi.org/10.4028/WWW.SCIENTIFIC.NET/MSF.1027.170

[7] D. Song, X. L. Xiao, and G Li. et al. "Modeling and control strategy of a haptic interactive robot based on a cable-driven parallel mechanism." Mechanical Sciences, vol.14, no.1, pp.19-32, 2023, https://doi.org/10.5194/MS-14-19-2023

[8] X. Y. Peng, et al. "Modelling and RBF Control of Low-Limb Swinging Dynamics of a Human–Exoskeleton System." Actuators, vol.12, no.9, pp.353-, 2023, https://doi.org/10.3390/ACT12090353

[9] D. Y. Yu. "Kinematic Parameter Identification for a Parallel Robot with an Improved Particle Swarm Optimization Algorithm." Applied Sciences, vol.14, no.15, pp.6557-6557, 2024, https://doi.org/10.3390/APP14156557

[10] Y. Bai, and S. J. Hsieh. "A hybrid method using FABRIK and custom ANN in solving inverse kinematic for generic serial robot manipulator." The International Journal of Advanced Manufacturing Technology, vol.130, no.9-10, pp.4883-4904, 2024, https://doi.org/10.1007/S00170-023-12928-3

[11] J. Zhou, et al. "Human–Robot Cooperation Control Strategy Design Based on Trajectory Deformation Algorithm and Dynamic Movement Primitives for Lower Limb Rehabilitation Robots." Processes, vol.12, no.5, 2024, https://doi.org/10.3390/PR12050924

[12] H. Li, and L. Z. Cao. "ANALYSIS AND SIMULATION OF HUMAN DYNAMICS IN FIGURE SKATING SPORTS." Journal of Mechanics in Medicine and Biology prepublish, 2024, https://doi.org/10.1142/S0219519424400542

[13] Z. W. Shi, et al. "Analysis of the CPZ/Wnt4 osteogenic pathway for high-bonding-strength composite-coated magnesium scaffolds through transcriptomics." Materials Today Bio, vol.28, pp.101234-101234, 2024, https://doi.org/10.1016/J.MTBIO.2024.101234

[14] L. H. Yao, H. L. Qin, and Deyong Xian, et al. "A research on low-earth-orbit signal-of-opportunity interference suppression algorithm based on adaptive signal iterative subspace projection technique." Frontiers in Physics, vol.13, pp.1557330-1557330, 2025, https://doi.org/10.3389/FPHY.2025.1557330

[15] J. Shi, Y. Xia, Z. Luan, Z. Xu, B. Wang, and T. Liu. "Kinematics analysis of parallel rope traction skating training robot." Metalurgija, Volume 65, Issue 3, 2026, https://doi.org/10.64486/m.65.3.4

[16] B. H. Wang, H. Y. Shi, et al. "Research on real-time kinematics algorithm and gait planning of rope-driven skating training robot." archive of mechanical engineering, 2025, vol. 72, no. 4, pp. 765–793, https://doi.org/10.24425/ame.2025.155872

[17] H.Y. Tong, F. Y. Zhang, and Y. K Zhai, et al. "Microstructure and Properties of Plasma Cladding Fe/Ni-WC Gradient Composite Coating on 65Mn Steel." Journal of Thermal Spray Technology prepublish, pp.1-14. 2025. https://doi.org/10.1007/S11666-025-02054-9

[18] S. Li, et al. "Study on the Corrosion Resistance of Laser Remelting/Diamond-Like Carbon Composite Coatings on Stainless Steel Surface." Journal of Materials Engineering and Performance, vol.35, no.2, pp.1-11, 2025, https://doi.org/10.1007/S11665-025-11618-3

[19] M. Andrea; R. Gabriele, C. Andrea, and L. Alessandro. "Muscle Fatigue Assessment in Healthcare Application by Using Surface Electromyography: A Transfer Learning Approach." Sensors, vol.26, no.2, pp.654-654, 2026, https://doi.org/10.3390/S26020654

[20] J. M. R. Martı´nez, and B. Ravani. "On Mobility Analysis of Linkages Using Group Theory." Journal of Mechanical Design, vol.125, no.1, pp.70-80, 2003, https://doi.org/10.1115/1.1541628

[21] C. X. Liu, et al. " Robust adaptive dynamic control of electromagnetically actuated soft-tethered robots for medical intervention." Control Engineering Practice, vol.153, pp.106107-106107, 2024, https://doi.org/10.1016/J.CONENGPRAC.2024.106107